Article

Water Penetration Profile at the Protein-Lipid Interface in Na,K-ATPase Membranes

Rosa Bartucci,[1] Rita Guzzi,[1] Mikael Esmann,[2] and Derek Marsh[3,*]

[1]Department of Physics, Molecular Biophysics Laboratory and CNISM Unit, University of Calabria, Ponte P. Bucci, Cubo 31C, 87036 Rende (CS), Italy; [2]Department of Biomedicine, Aarhus University, 8000 Aarhus, Denmark; and [3]Max-Planck-Institut für biophysikalische Chemie, 37070 Göttingen, Germany

ABSTRACT The affinity of ionized fatty acids for the Na,K-ATPase is used to determine the transmembrane profile of water penetration at the protein-lipid interface. The standardized intensity of the electron spin echo envelope modulation (ESEEM) from ^{2}H-hyperfine interaction with D_2O is determined for stearic acid, *n*-SASL, spin-labeled systematically at the C-*n* atoms throughout the chain. In both native Na,K-ATPase membranes from shark salt gland and bilayers of the extracted membrane lipids, the D_2O-ESEEM intensities of fully charged *n*-SASL decrease progressively with position down the fatty acid chain toward the terminal methyl group. Whereas the D_2O intensities decrease sharply at the $n = 9$ position in the lipid bilayers, a much broader transition region in the range $n = 6$ to 10 is found with Na,K-ATPase membranes. Correction for the bilayer population in the membranes yields the intrinsic D_2O-intensity profile at the protein-lipid interface. For positions at either end of the chains, the D_2O concentrations at the protein interface are greater than in the lipid bilayer, and the positional profile is much broader. This reveals the higher polarity, and consequently higher intramembrane water concentration, at the protein-lipid interface. In particular, there is a significant water concentration adjacent to the protein at the membrane midplane, unlike the situation in the bilayer regions of this cholesterol-rich membrane. Experiments with protonated fatty acid and phosphatidylcholine spin labels, both of which have a considerably lower affinity for the Na,K-ATPase, confirm these results.

INTRODUCTION

Lipid probes spin labeled at specific molecular positions have proved extremely effective in mapping the transbilayer polarity profile that constitutes the permeability barrier of biological membranes to polar molecules and ions (see, e.g. (1,2)). A variety of electron paramagnetic resonance (EPR) parameters are available to characterize the environmental polarity. These include hyperfine couplings in conventional EPR (3–5), *g*-values in high-field EPR (6), relaxation enhancement by molecular oxygen (7–9), and direct detection of penetrant water by pulsed EPR (10,11).

In lipid bilayers, the EPR-determined permeation barrier assumes a sigmoidal form with a relatively sharp transition to the apolar interior of the membrane. Transbilayer profiles of this type have now been characterized in detail for many cases (see, e.g. (1,12,13–18)). Furthermore, nonlinear and pulsed EPR have been used to characterize the polarity of fatty acid binding pockets in soluble proteins (19–21). Far less is known, however, about the transmembrane polarity profile at the interface between the transmembrane segments of integral proteins and the lipid bilayer. This is a region of potential functional interest because it can provide a sink for the permeation of polar solutes, is the point of access to the substrate binding site of lipolytic enzymes and to the sites of both active and facilitated phospholipid flip-flop, and is also the location of the gate for release of nascent transmembrane peptides from the translocon.

Here, we use pulse-EPR spectroscopy of lipids spin labeled at specific positions in the fatty acid chain to determine the transverse polarity profile at the protein-lipid interface in Na,K-ATPase membranes. Modulation of the electron spin-echo envelope (ESEEM) by hyperfine interaction with the ^{2}H-nucleus of D_2O is a direct measure of the water concentration in the vicinity of the spin-label group. Previously established patterns of lipid selectivity for interaction with the Na,K-ATPase (22) are used to isolate the contribution from the protein-lipid interface to the transmembrane polarity.

MATERIALS AND METHODS

Materials

Stearic acids spin labeled at the C-*n* position of the chain, *n*-SASL [*n*-(4,4-dimethyloxazolidine-*N*-oxyl) stearic acid], and the corresponding phosphatidylcholines with *n*-SASL acylated at the *sn*-2 position (*n*-PCSL), were synthesized as described in (23,24).

Preparation of shark salt gland Na,K-ATPase

Na,K-ATPase from the rectal gland of *Squalus acanthias* was prepared as described previously (25) but omitting the treatment with saponin.

Submitted April 8, 2014, and accepted for publication July 30, 2014.

*Correspondence: dmarsh@gwdg.de

Editor: David Cafiso.

0006-3495/14/09/1375/8 $2.00

http://dx.doi.org/10.1016/j.bpj.2014.07.057

The Na,K-ATPase constituted typically ~70% of the total protein and the specific Na,K-ATPase activity was 1650 μmol of ATP hydrolyzed per mg protein per hour (26). The enzyme is stable over the pH range 5.2−9.2 at low temperatures in the absence of salt (27); at higher temperatures, inactivation is inhibited by addition of salt (28). Membrane lipids were extracted with $CHCl_3/CH_3OH$ (2:1 v/v) as described in (29).

Transfer of Na,K-ATPase membranes to D_2O-containing media

Before addition of the spin-labeled lipids, the Na,K-ATPase membranes were pelleted by centrifugation at 220,000 × *g* for 60 min at 10°C. The pellets were taken up in a buffer containing 11.1 mM Tris, 11.1 mM CDTA, and 55 mM NaCl, pH 7.0 (made in 99.8% D_2O) and kept at 14°C for 60 min. These membranes were pelleted by centrifugation at 130,000 × *g* for 120 min at 14°C. The pellets were taken up in the same D_2O buffer and incubated overnight at 14°C. These membranes were then pelleted by centrifugation at 130,000 × *g* for 120 min at 14°C. Pellets after this centrifugation were taken up in a buffer containing 10 mM Tris and 1 mM CDTA (in 99.8% D_2O) at pH 6.1, 7.0 or 8.9. The membranes were kept at 14°C for 60 min and then pelleted by centrifugation at 130,000 × *g* for 120 min at 14°C. The resulting pellet was taken up in the same buffer at a concentration of ~10 mg protein/ml. The H_2O concentration was <0.3% at this stage.

Spin labeling of Na,K-ATPase membranes

Membranes were spin labeled by addition of 5 μl of concentrated *n*-SASL (or *n*-PCSL) solution in EtOH to 0.5 ml of membrane suspension (10 mg protein/ml) giving spin label/protein ratios (w/w) of 1/100 or 1/50. After incubation for 150 min at 14°C, the membranes were pelleted by centrifugation at 220,000 × *g* for 60 min at 14°C. The pellets were then transferred to 3-mm EPR tubes and stored at −18°C.

Spin labeling of extracted lipid membranes

Extracted lipids in $CHCl_3$/MeOH (2:1 v/v) were codissolved with 0.5 mol % of *n*-SASL in chloroform. The solvent was evaporated by placing the sample first in a stream of dry nitrogen and then under vacuum overnight. The dried lipids were finally dispersed at a concentration of 1 mg/ml in D_2O buffer at pH 8.9 (or in the same buffer as used for the Na,K-ATPase membrane preparation) by periodically vortexing and mixing at 45°C. The hydrated lipid bilayers were transferred to a standard 3-mm quartz EPR tube, concentrated by pelleting in a benchtop centrifuge, and stored at −18°C until use.

EPR spectroscopy

Pulsed EPR data were collected at 77 K on an ELEXSYS E580 9-GHz Fourier Transform FT-EPR spectrometer (Bruker Biospin, Rheinstetten, Germany) equipped with an MD5 dielectric resonator and a CF 935P cryostat (Oxford Instruments, UK). To obtain ESEEM spectra, three-pulse, stimulated echo ($\pi/2-\tau-\pi/2-T-\pi/2-\tau-$echo) decays were collected by using microwave pulse widths of 12 ns, with the microwave power adjusted to give $\pi/2$-pulses. The time delay T between the second and the third pulses was incremented from $T_o = 20$ ns by $N = 700$ steps of $\Delta T = 12$ ns, while maintaining the separation τ between the first and the second pulses constant at 168 ns. This value of τ simultaneously maximizes the ESEEM signals from deuterium and protons (30). A four-step phase-cycling program, $+(x,x,x)$, $-(x,-x,x)$, $-(-x,x,x)$, $+(-x,-x,x)$, where the initial sign indicates the phase of the detection ($\pm y$), was used to eliminate unwanted echoes (31).

The time-dependent echo amplitudes, $V(\tau,T)$, were processed to yield standardized ESEEM intensities, according to the protocol developed previously (30,32). The average experimental echo decay, $\langle V(\tau,T)\rangle$, was obtained by fitting $V(\tau,T)$ vs. T with a biexponential function. The normalized ESEEM signal was then obtained as

$$V_{norm}(\tau,T) = V(\tau,T)/\langle V(\tau,T)\rangle - 1. \quad (1)$$

A complex Fourier transform of this normalized time-domain signal is evaluated numerically:

$$I(\omega_k) = \Delta T \sum_{j=0}^{N} V_{norm}(\tau, T_o + j\Delta T) \times \exp(-i\omega_k(\tau + T_o + j\Delta T)), \quad (2)$$

where $\omega_k = 2\pi k/(N\Delta T)$ with $k = -N/2$ to $+N/2$. The real and imaginary Fourier coefficients are then used to obtain the absolute-value ESEEM spectrum. Note that the discrete Fourier transform software supplied with the ELEXSYS FT-EPR spectrometer does not take account of different dwell times, ΔT, in determining amplitudes of the ESEEM spectrum. Definition according to Eq. 2 provides machine-independent spectral densities, with the dimensions of time, which can be used for quantitative comparison of different D_2O-containing systems (32), e.g., native membranes and bilayers of the extracted membrane lipids.

Conventional continuous wave (CW)-EPR spectra were recorded on an ESP-300 spectrometer (Bruker) operating at 9 GHz with 100-kHz field modulation and equipped with an ER 4111VT temperature controller.

RESULTS

It is known from studies of lipid-protein interactions with conventional spin-label EPR (27,33) that fully ionized fatty acids display a high affinity for interaction with the Na,K-ATPase, as compared with a background membrane lipid such as phosphatidylcholine. Consequently, ESEEM intensities of negatively charged spin-labeled fatty acids in native Na,K-ATPase membranes contain a strong contribution from D_2O in the vicinity of the protein interface, in addition to the background contribution from the spin-labeled fatty acid in the lipid bilayer regions of the membrane. Measurements are therefore performed with positional isomers of *n*-SASL at pH 8.9, for which the carboxyl group is fully dissociated, even in the lower polarity environment at the membrane surface (34).

ESEEM spectra

Fig. 1 shows the low-frequency region in the absolute-value ESEEM spectra of ionized spin-labeled *n*-SASL, in native Na,K-ATPase membranes and in bilayer dispersions of the extracted membrane lipids. The membranous samples are suspended in D_2O buffer at pH 8.9; spectra are given for different positions, *n*, of the spin label in the fatty acid chain. All ESEEM spectra consist of a peak at the ^{2}H-Larmor frequency of ~2.6 MHz that arises from D_2O in the vicinity of the spin-label group and a peak at the ^{1}H-Larmor frequency of 14.6 MHz that arises from matrix protons and serves as an

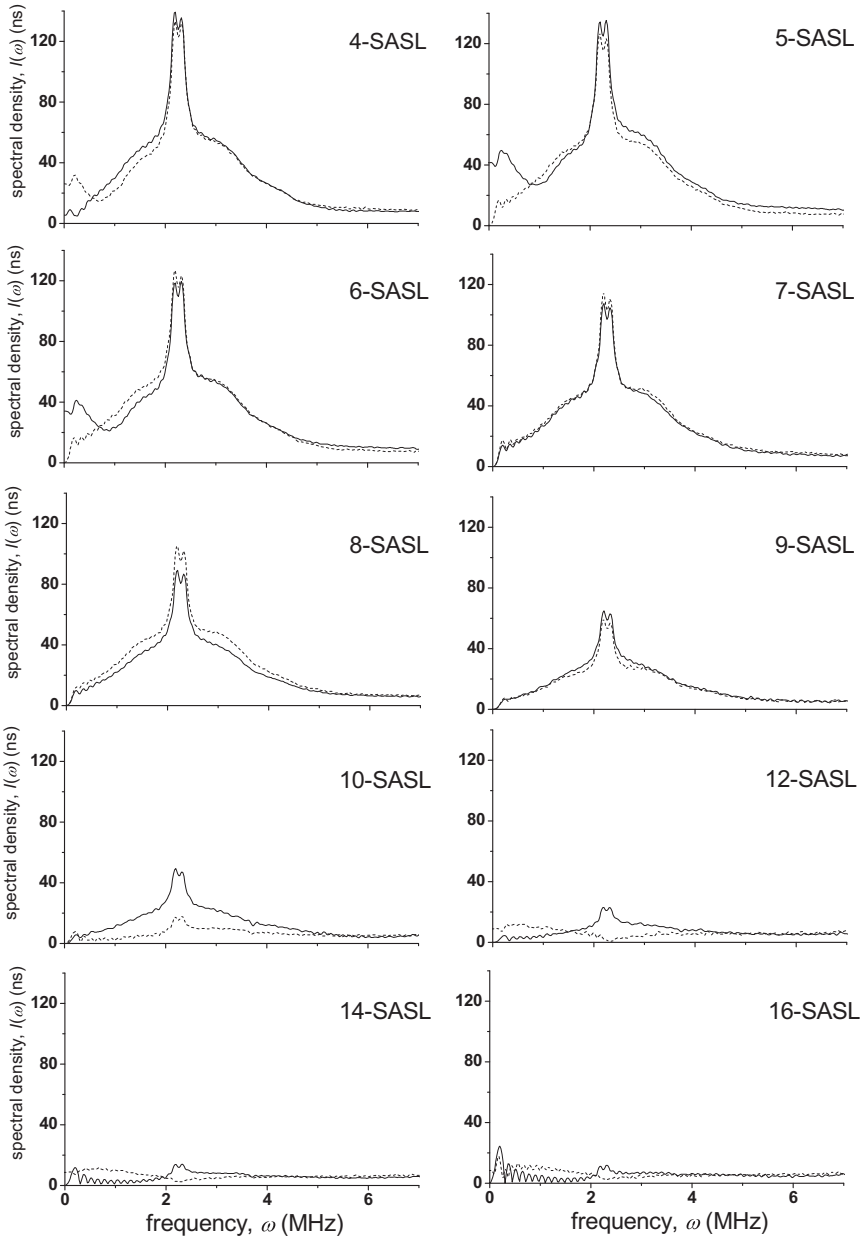

FIGURE 1 Absolute-value Fourier-transform D_2O-ESEEM spectra of stearic acid (*n*-SASL), spin labeled at the C-*n* position, in native Na,K-ATPase membranes from *Squalus acanthias* (*solid lines*) or in bilayer membranes of the extracted membrane lipids (*dashed lines*) dispersed in D_2O buffer at pH 8.9.

additional internal standard for the D_2O intensity (see Fig. S1 in the Supporting Material). The D_2O peak of each spectrum consists of a broad component that arises from D_2O molecules that are hydrogen bonded to the nitroxide and a narrow component that corresponds to D_2O molecules that are not hydrogen bonded to the –NO group but are located in the vicinity of the spin-label site (30). As seen from Fig. 1, the ratio of the broad to narrow components remains approximately constant with label position. The mean value is $I_{broad}/I_{narrow} = 0.72 \pm 0.08$ for membranes and 0.72 ± 0.04 for the lipids. These values are comparable to those for a water exposed surface label, e.g., Class I groups of the Na,K-ATPase for which $I_{broad}/I_{narrow} = 0.70$ (35) and a surface residue on human serum albumin with $I_{broad}/I_{narrow} = 0.65$ (20).

In all cases, the D_2O-ESEEM intensities decrease with position of the spin label down the fatty acid chain toward the membrane midplane. For a given spin-label position, the D_2O-amplitudes are greater in native Na,K-ATPase membranes than in bilayer membranes of the extracted lipids, except for some intermediate positions. This corresponds to an increased average water concentration in the protein-containing membranes, relative to membranes of the lipid alone. Note that, in principle, ^2H-ESEEM intensity can arise from exchangeable protons in the protein side chains. We would expect this to augment the narrow component from non-H-bonded spin labels. The I_{broad}/I_{narrow} ratio would then be reduced for membranes, relative to lipids, which is not the case (see Fig. S2).

Transmembrane water profiles

Fig. 2 gives the positional profile of the standardized total intensities, I, of the D_2O-ESEEM spectrum for the two different membranous samples. For the lipid bilayer membranes, the profile is sigmoidal with a sharp transition to the apolar interior of the membrane at $n \approx 9$, which closely resembles the behavior already found in synthetic phosphatidylcholine-cholesterol mixtures (1,30). As seen from Fig. 2, the form of this intensity profile, $I(n)$, is well described by the Boltzmann sigmoid that was used previously (1):

$$I(n) = \frac{I_1 - I_2}{1 + \exp((n - n_o)/\lambda)} + I_2, \quad (3)$$

where I_1 and I_2 are the limiting values of I at the polar headgroup and terminal methyl ends of the chain, respectively, n_o is the value of n at the point of maximum gradient, corresponding to $I(n_o) = (I_1+I_2)/2$, and λ is an exponential decay length. The significance of Eq. 3 is that it corresponds to a two-compartment distribution between outer ($n < n_o$) and inner ($n > n_o$) regions of the membrane, in which the free energy of transfer, $(n-n_o)k_BT/\lambda$, increases linearly with distance, $n-n_o$, from the dividing plane. Mostly, reproducibility of the intensity measurements is comparable to the size of the symbols in Fig. 2 (and Fig. 3), except in the steeply changing region of the profile. In particular, duplicates confirm the absence of D_2O-ESEEM intensity at positions $n = 12-16$ in the lipids, as found also for model membranes with similarly high cholesterol content (30).

Compared with the lipid bilayers, the D_2O profile of the native Na,K-ATPase membranes has a much broader transition that takes place over the range $n \approx 6-10$, and has larger intensities for a given value of n at both ends of the transition. This can be attributed to the higher polarity, and consequently higher water concentration, at the protein-lipid interface than in the lipid bilayer regions of the membrane. The net D_2O intensity in the membrane, I_m, is the weighted average of that in the bilayer regions of the membrane, I_f, and that at the protein interface, I_b: i.e., $I_m = f_bI_b + (1 - f_b)I_f$, where f_b is the fraction of lipids at the protein interface. The latter is known from conventional spin-label EPR studies of lipid-protein interactions in Na,K-ATPase membranes: $f_b = 0.43$ for ionized stearic acid at pH 8.9 (27).

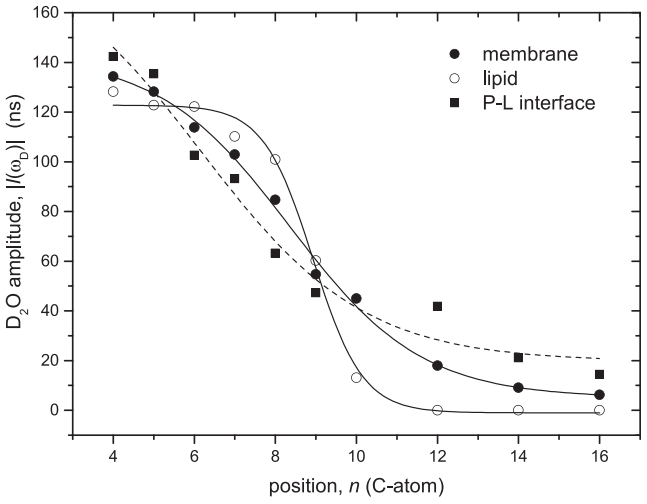

FIGURE 2 Dependence of D_2O-ESEEM amplitudes on position, n, in the chain of ionized spin-labeled stearic acid (n-SASL) at pH 8.9: in Na,K-ATPase membranes (*solid circles*, I_m) and in bilayer membranes of the extracted lipids (*open circles*, I_f). Solid squares are the D_2O-amplitudes at the protein-lipid interface, I_b, that are calculated from the membrane and lipid data according to Eq. 4. Lines are fits of a Boltzmann sigmoidal profile according to Eq. 3.

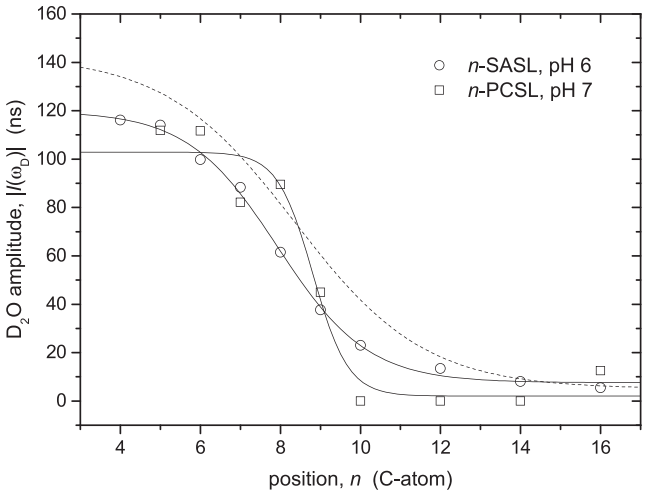

FIGURE 3 Dependence of D_2O-ESEEM amplitudes on position, n, in the chain of protonated spin-labeled stearic acid (n-SASL) at pH 6.1 (*open circles*), and of spin-labeled phosphatidylcholine (n-PCSL) at pH 7.0 (*open squares*), in Na,K-ATPase membranes. The dependence for ionized stearic acid in Na,K-ATPase membranes at pH 8.9 is given by the dashed line (cf. Fig. 2). Solid lines are fits of Eq. 3 to the data points for n-SASL (pH 6.1) and n-PCSL, respectively.

The intrinsic D_2O-intensity profile at the protein-lipid interface (I_b) may therefore be obtained from ESEEM measurements on the native membranes and extracted lipids (I_m and I_f, respectively):

$$I_b = \frac{I_m - I_f}{f_b} + I_f, \quad (4)$$

where f_b is obtained from spectral subtractions with the conventional EPR spectra (27). This profile for the lipid-protein interface is given by the solid squares and dashed line in Fig. 2. It is broader than the average profile obtained from native membranes, and is characterized by considerably higher D_2O intensities in the mid-region of the membrane. Parameterization of the profile for the protein-lipid interface according to Eq. 3, is compared with that for the lipid bilayer regions and for the native membranes in Table 1. The protein-lipid interface is characterized by a much longer decay length λ, and higher

TABLE 1 Parameters specifying the transmembrane water profiles in Fig. 2, according to Eq. 3

	I_1 (ns)	I_2 (ns)	n_o	λ
Lipid	122.8 ± 2.5	−1.0 ± 2.6	8.93 ± 0.08	0.61 ± 0.07
P-L interface	189 ± 61	19.6 ± 8.2	6.2 ± 1.6	2.0 ± 0.9
Membrane	142.9 ± 5.5	5.0 ± 2.9	8.4 ± 0.2	1.6 ± 0.2

overall D_2O-amplitudes I_1 and I_2, relative to lipid-bilayer membranes (1).

Comparison with phosphatidylcholine and protonated fatty acid

All the studies above have been conducted with negatively charged fatty acid spin labels. Uncharged (i.e., protonated) fatty acids and zwitterionic phosphatidylcholine display a much lower affinity for the Na,K-ATPase (22,27). Thus, *n*-SASL at low pH and *n*-PCSL will display ESEEM spectra with a greater contribution from the bilayer regions of the membrane, relative to *n*-SASL at high pH.

Fig. 3 gives the positional profiles of the standardized total intensities, I, of the D_2O-ESEEM spectrum for *n*-SASL at pH 6.1, and for *n*-PCSL, in native Na,K-ATPase membranes. For comparison, the profile of *n*-SASL at pH 8.9 is given by the dashed line in Fig. 3. For both the uncharged fatty acid and the zwitterionic phosphatidylcholine, the D_2O-amplitudes are less than those for the negatively charged fatty acid, which has a larger fractional population at the protein-lipid interface. The values of f_b are 0.22 and 0.21 for protonated *n*-SASL and *n*-PCSL, respectively, compared with $f_b = 0.43$ for ionized *n*-SASL (27). Thus, measurements with both *n*-SASL at pH 6.1 and *n*-PCSL confirm that the water concentration, and hence polarity, is higher at the protein-lipid interface than in the lipid bilayer regions of the membranes. A more quantitative comparison with the *n*-SASL data at pH 8.9, is not appropriate because the vertical location of the spin label differs between the three cases (see, e.g., (34)).

^{14}N-hyperfine splittings

The ^{14}N-hyperfine splittings in the conventional CW EPR spectra are sensitive to environmental polarity, including the presence of nonbonded and hydrogen-bonded water (2,36). Fig. 4 gives the dependence on spin-label chain position for the outer hyperfine splitting, $2A_{zz}$, of ionized *n*-SASL in Na,K-ATPase membranes (*solid circles*) and bilayers of the extracted membrane lipids (*open circles*). The spectra are recorded at 77 K, where librational motion is absent. The positional dependences of the outer hyperfine splittings, and the differences between membranes and extracted lipids, therefore are attributable to polarity alone. It is seen that the positional dependences of the hyperfine splittings in Fig. 4 are very similar to those of the D_2O-amplitudes in Fig. 2. A sigmoidal form is observed for

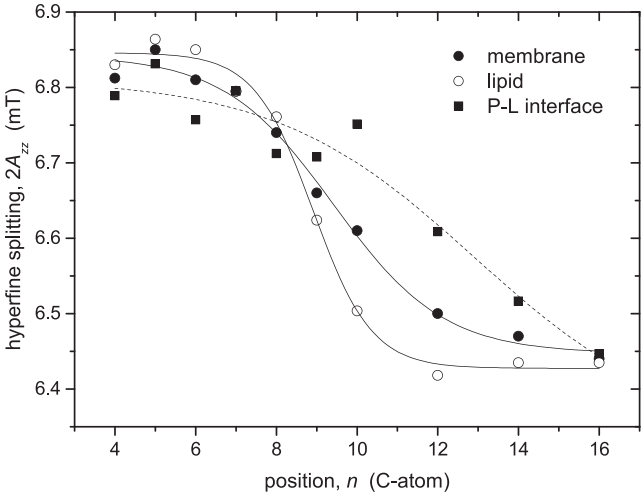

FIGURE 4 Dependence of the outer hyperfine splitting, $2A_{zz}$, on position, *n*, in the chain of ionized spin-labeled stearic acid (*n*-SASL) at pH 8.9: in Na,K-ATPase membranes (*solid circles*) and in bilayer membranes of the extracted lipids (*open circles*). Solid squares are the outer hyperfine splittings at the protein-lipid interface that are calculated from the membrane and lipid data according to Eq. 5. Lines are fits of a Boltzmann sigmoidal profile according to Eq. 3.

both extracted lipids and membranes, and the sigmoid is sharper in lipid bilayers than in membranes. Furthermore, the polarity registered by A_{zz} toward the terminal methyl end of the lipid chain is higher in the membranes than in lipid bilayers, although this is not the case at the carboxyl end.

In principle, the response of spin-label hyperfine splittings to polarity is complex, depending on both local reaction fields and the extent of hydrogen bonding to the nitroxide (2). To a certain degree of approximation, however, one can assume that polarity contributions to A_{zz} are additive and that contributions of the protein-lipid interface to the net hyperfine splitting of membranes may be approximated by a relation analogous to Eq. 4:

$$A_{zz,b} = \frac{A_{zz,m} - A_{zz,f}}{f_b} + A_{zz,f}, \tag{5}$$

where the subscripts *b*, *m*, and *f* again represent protein-lipid interface, membrane and lipid bilayer, respectively. The values of $2A_{zz}$ for the protein-lipid interface, corrected in this way are given by the solid squares in Fig. 4. In common with Fig. 2, these values imply a less steep polarity profile than that offered by the bilayer permeability barrier.

DISCUSSION

The transmembrane profile of water concentration, as registered by the negatively charged fatty acid, differs markedly in native Na,K-ATPase membranes from that in bilayer membranes of the extracted membrane lipids (Fig. 2). This arises from the higher environmental polarity at the

protein-lipid interface, relative to that in the lipid-regions of the membrane (see also Fig. 4). Correction for the bilayer contribution to the membrane ESEEM spectra yields the local water concentration profile at the protein-lipid interface (Eq. 4 and Fig. 2). The profile in the bilayer regions exhibits a sharp sigmoidal form that is found with synthetic lipid membranes (30) containing similarly high contents of cholesterol (33). In comparison, the profile at the protein-lipid interface is characterized by higher water concentrations in the chain regions both close to the lipid headgroups and at the middle of the membrane, and a much more gradual decrease between these two regions, than in bilayer regions of the membrane. For the latter reason, the water concentration at intermediate chain positions ($n = 6-8$) can actually be somewhat higher in the bilayer than at the protein-lipid interface.

It is instructive to compare the intramembrane water accessibilities at the protein-lipid interface with those in the ligand sites of classical fatty acid-binding proteins, such as serum albumin and β-lactoglobulin. For human serum albumin, the standardized D_2O-ESEEM intensities of spin-labeled fatty acids in the binding site are in the range 100−150 ns depending on chain position, whereas a value of 240 ns is found for a spin label covalently attached at the protein surface (20). The values for the fatty acid bound to serum albumin correspond to the upper part of the chain at the protein-lipid interface in Na,K-ATPase membranes (see Fig. 2). D_2O-ESEEM intensities of fatty acids bound to β-lactoglobulin are in the range 220−110 ns, decreasing with spin-label position down to C-12 of the chain (21). These values again correspond with the more polar regions of the protein-lipid interface in Na,K-ATPase membranes. However, it appears that the spin-label group does not enter fully into the binding pocket of β-lactoglobulin (21), which is less exposed to water than are the binding sites of serum albumin. The upper part of the chain at the protein-lipid interface therefore corresponds to the entrance of the hydrophobic binding pocket in β-lactoglobulin. Note also that the standardized D_2O-ESEEM intensity of spin labels bound to superficial −SH groups (Class I) of the Na,K-ATPase is ~220 ns, whereas that for the −SH groups essential to activity (Class II) is ~160 ns (35,37). The latter value is again comparable to the more polar regions of the chains at the protein-lipid interface. Approximately 60% of the spin intensity of Class II –SH groups remains associated with the membrane after removal of the extramembrane sector by extensive trypsinization (38). Cysteine residues Cys^{809}, Cys^{971}, and Cys^{990} are located at the lipid-protein interface in the crystal structure of the shark enzyme (39), and therefore are expected to have a D_2O-ESEEM intensity similar to that found here for lipids at the protein interface. The Class II groups that are removed by trypsin are presumably buried within the protein structure so as to give a water accessibility comparable to that at the lipid-protein interface. A good candidate for one of the latter is Cys^{428} that is essential to activity and close to the nucleotide binding site (35).

The polarity at the protein-lipid interface may also be deduced from the crystal structure of the Na,K-ATPase. Fig. 5 shows the overall structure of the shark salt gland Na,K-ATPase protein complex (Protein Data Bank (PDB) code: 2ZXE; (39)) with emphasis on the amino acid residues in contact with the lipid bilayer. These 243 residues were selected using the Orientations of Proteins in Membranes (OMP) database (40,41), and the residue numbers are given in the legend to Fig. 5, for the 10 transmembrane peptides of the α-subunit as well as the single peptides of the β- and γ-subunits. The hydrophobicity of the individual residues is assigned using the octanol scale established by Wimley and White (see (42,43)). A grayscale is used to indicate hydrophobicity, ranging from very high (Trp in *black*) to low hydrophobicity (*light gray* for Ala and *white* for Gly). With the representation given in Fig. 5, only residues at

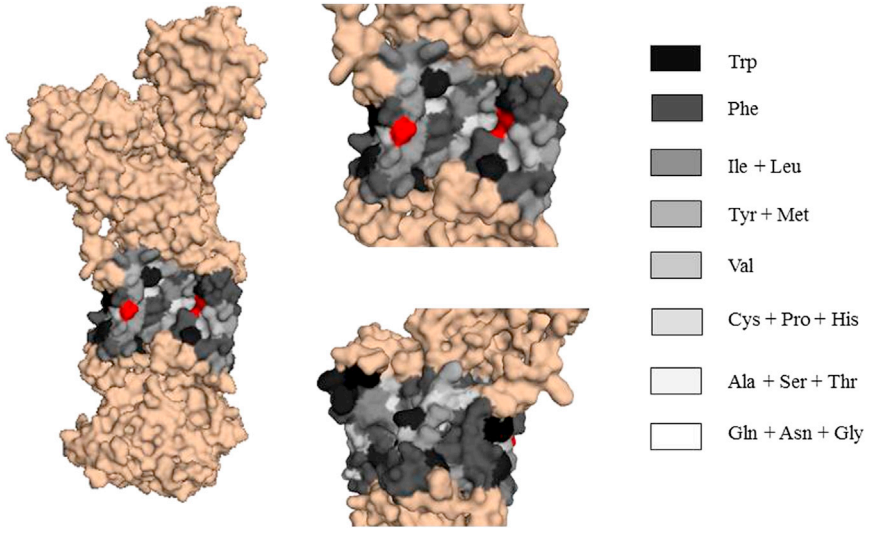

FIGURE 5 Crystal structure of shark salt gland Na,K-ATPase (PDB code: 2ZXE). Left: the entire protein; top right: intramembrane section expanded; bottom right: rotated by 180° about the membrane normal. Intramembrane parts are residues: 99−115, 129−149, 291−313, 320−344, 774−795, 804−822, 849−872, 917−937, 953−970, and 985−1001 (α-subunit); 33−61 (β-subunit); and 21−39 (γ-subunit) (40,41). All extramembrane residues are colored wheat. The grayscale reflects the hydrophobicity of the intramembrane residues (42,43). In the upper right panel, the red residue to the left is Thr-138, and that partly in a cavity to the right is Glu-960. Figure prepared with PyMOL (46). To see this figure in color, go online.

the surface of the protein are visible, i.e., those which interact with the bilayer lipids.

Only two residues in the central part of the membrane are of polar nature. These are shown in red in Fig. 5, with Thr-138 to the left and Glu-960 to the right in the upper right-hand panel. Inspection of the crystal structure reveals that the polar groups of these two residues do indeed protrude into the bilayer region. The remainder of the side chains that contain polar or charged groups (as defined by the OMP database, see legend to Fig. 5) are oriented with the polar part facing away from the lipid/protein interface.

The average hydrophobicity of the 131 residues facing the lipid is -3.36 kJ mol^{-1} when calculated using the octanol scale, which is much higher than the average hydrophobicity of -0.03 kJ mol^{-1} for the 112 residues that contribute to the interior of the transmembrane domain. For comparison, the mean hydrophobicity of the extramembrane sectors of the protein is $+1.20$ kJ mol^{-1}. Fig. 6 shows the hydrophobicity profile of the intramembrane surface calculated for 0.3-nm thick slices of the protein. There is a sharp increase in hydrophobic free energy of the protein on entering the membrane, but the hydrophobic profile at the lipid-protein interface within the membrane is very shallow (cf. also (44)). Qualitatively, this agrees with the experimental measurements of water penetration by ^{2}H-ESEEM and of intramembrane polarity reflected by the N-hyperfine coupling. The profile of both these quantities is far less steep at the protein interface than in lipid-bilayer regions of the membrane, and correspondingly the absolute values at the membrane midplane are higher at the protein than in the bilayer. Note that in (43), the large variance in the profile, such as we find in Fig. 6, is reduced by grouping together all structures from a given type of membrane.

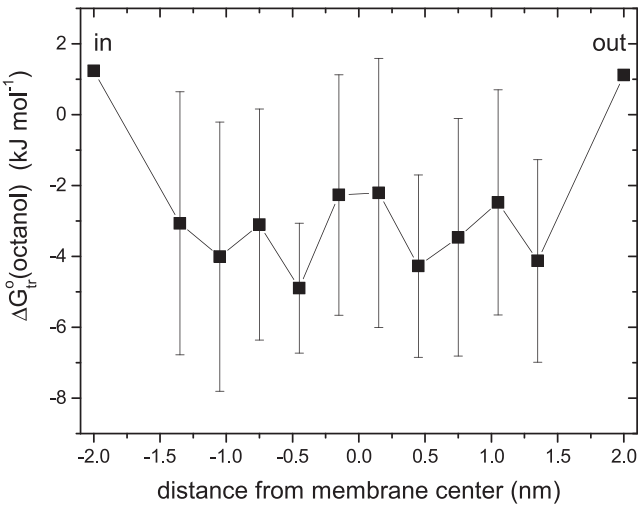

FIGURE 6 Hydrophobicity profile for the transmembrane sector of shark Na,K-ATPase. Mean free energy of transfer, ΔG^o_{tr}, from water to octanol (42,43) for lipid-facing amino acid residues is plotted against distance from the membrane midplane. "in" and "out" are mean values of ΔG^o_{tr} for all residues of the cytoplasmic and extracellular sectors, respectively.

Water accessibility at the protein-lipid interface of the reconstituted KcsA potassium channel has been studied by combining site-directed spin labeling with D_2O-ESEEM (45). Spin-labeled protein side chains were monitored, as opposed to the chains of the surrounding lipids studied here. Furthermore, the lipid composition was very different because cholesterol was absent, compared with the equimolar content of cytoplasmic membranes as here. The results have certain similarities with ours, but also clear differences. Residues with higher D_2O-ESEEM intensities than those of the lipid chains were found at the outer end of the lipid-exposed α-helix, but intensities toward the center of the transmembrane section were lower than for the lipids. A low intensity was found for a side chain located in a groove between transmembrane helices, which highlights possible differences from the surrounding chains. Additionally, the residue data scatters with position, unlike the chains, which might be anticipated from the variance in Fig. 6 and equivalent calculations for KcsA. Even so, the profile for the latter (PDB: 1BL8, not shown) does not have a higher hydrophobicity at the middle of the membrane. Overall, a detailed comparison of the experimental data is not possible because the normalized intensities in (45) are anomalously low relative to ours, for which we have no explanation. Furthermore, the shape of the lipid profile is very different from ours, which could reflect the different lipid composition.

To summarize our results, the polarity and concentrations of intramembrane water at the lipid interface with integral proteins are higher, and form less of an abrupt hydrophobic barrier, than is found in the lipid-bilayer regions of biological membranes. Certain similarities exist with the ligand sites of soluble fatty acid-binding proteins. These results have functional implications for membrane permeability in general (we expect the protein-lipid interface to constitute a passive sink), and specifically for the interaction of lipid substrates with lipolytic enzymes and membrane flippases. In the latter case, it is interesting to note that active translocation between the inner and outer lipid leaflets is mediated by members of the P4 subfamily of P-type ATPases, of which Na,K-ATPase is an archetypical example.

SUPPORTING MATERIAL

Two figures are available at http://www.biophysj.org/biophysj/supplemental/S0006-3495(14)00804-2.

REFERENCES

1. Marsh, D. 2001. Polarity and permeation profiles in lipid membranes. *Proc. Natl. Acad. Sci. USA*. 98:7777–7782.

2. Marsh, D. 2010. Spin-label EPR for determining polarity and proticity in biomolecular assemblies: transmembrane profiles. *Appl. Magn. Reson.* 37:435–454.

3. Griffith, O. H., P. J. Dehlinger, and S. P. Van. 1974. Shape of the hydrophobic barrier of phospholipid bilayers (evidence for water penetration in biological membranes). *J. Membr. Biol.* 15:159–192.
4. Pates, R. D., and D. Marsh. 1987. Lipid mobility and order in bovine rod outer segment disk membranes. A spin-label study of lipid-protein interactions. *Biochemistry.* 26:29–39.
5. Subczynski, W. K., A. Wisniewska, …, A. Kusumi. 1994. Hydrophobic barriers of lipid bilayer membranes formed by reduction of water penetration by alkyl chain unsaturation and cholesterol. *Biochemistry.* 33:7670–7681.
6. Kurad, D., G. Jeschke, and D. Marsh. 2003. Lipid membrane polarity profiles by high-field EPR. *Biophys. J.* 85:1025–1033.
7. Subczynski, W. K., J. S. Hyde, and A. Kusumi. 1989. Oxygen permeability of phosphatidylcholine—cholesterol membranes. *Proc. Natl. Acad. Sci. USA.* 86:4474–4478.
8. Subczynski, W. K., J. S. Hyde, and A. Kusumi. 1991. Effect of alkyl chain unsaturation and cholesterol intercalation on oxygen transport in membranes: a pulse ESR spin labeling study. *Biochemistry.* 30:8578–8590.
9. Dzikovski, B. G., V. A. Livshits, and D. Marsh. 2003. Oxygen permeation profile in lipid membranes: comparison with transmembrane polarity profile. *Biophys. J.* 85:1005–1012.
10. Bartucci, R., R. Guzzi, …, L. Sportelli. 2003. Intramembrane polarity by electron spin echo spectroscopy of labeled lipids. *Biophys. J.* 84:1025–1030.
11. Bartucci, R., D. A. Erilov, …, D. Marsh. 2006. Time-resolved electron spin resonance studies of spin-labelled lipids in membranes. *Chem. Phys. Lipids.* 141:142–157.
12. Fretten, P., S. J. Morris, …, D. Marsh. 1980. Lipid-lipid and lipid-protein interactions in chromaffin granule membranes. A spin label ESR study. *Biochim. Biophys. Acta.* 598:247–259.
13. Swamy, M. J., M. Ramakrishnan, …, D. Marsh. 2000. Spin-label electron spin resonance studies on the mode of anchoring and vertical location of the *N*-acyl chain in *N*-acylphosphatidylethanolamines. *Biochemistry.* 39:12476–12484.
14. Schorn, K., and D. Marsh. 1996. Lipid chain dynamics and molecular location of diacylglycerol in hydrated binary mixtures with phosphatidylcholine: spin label ESR studies. *Biochemistry.* 35:3831–3836.
15. Rama Krishna, Y. V. S., and D. Marsh. 1990. Spin label ESR and ^{31}P-NMR studies of the cubic and inverted hexagonal phases of dimyristoylphosphatidylcholine/myristic acid (1:2, mol/mol) mixtures. *Biochim. Biophys. Acta.* 1024:89–94.
16. Bartucci, R., A. Gambacorta, …, L. Sportelli. 2005. Bipolar tetraether lipids: chain flexibility and membrane polarity gradients from spin-label electron spin resonance. *Biochemistry.* 44:15017–15023.
17. Hoffmann, P., K. Sandhoff, and D. Marsh. 2000. Comparative dynamics and location of chain spin-labelled sphingomyelin and phosphatidylcholine in dimyristoyl phosphatidylcholine membranes studied by EPR spectroscopy. *Biochim. Biophys. Acta.* 1468:359–366.
18. Marsh, D., B. G. Dzikovski, and V. A. Livshits. 2006. Oxygen profiles in membranes. *Biophys. J.* 90:L49–L51.
19. Livshits, V. A., and D. Marsh. 2000. Fatty acid binding sites of serum albumin probed by non-linear spin-label EPR. *Biochim. Biophys. Acta.* 1466:350–360.
20. De Simone, F., R. Guzzi, …, R. Bartucci. 2007. Electron spin-echo studies of spin-labelled lipid membranes and free fatty acids interacting with human serum albumin. *Biochim. Biophys. Acta.* 1768:1541–1549.
21. Guzzi, R., B. Rizzuti, and R. Bartucci. 2012. Dynamics and binding affinity of spin-labeled stearic acids in β-lactoglobulin: evidences from EPR spectroscopy and molecular dynamics simulation. *J. Phys. Chem. B.* 116:11608–11615.
22. Esmann, M., and D. Marsh. 2006. Lipid-protein interactions with the Na,K-ATPase. *Chem. Phys. Lipids.* 141:94–104.
23. Marsh, D. 2008. Electron spin resonance in membrane research: protein-lipid interactions. *Methods.* 46:83–96.
24. Marsh, D., and A. Watts. 1982. Spin-labeling and lipid-protein interactions in membranes. *In* Lipid-Protein Interactions, *Vol. 2*. Jost, P. C., and O. H. Griffith, editors. Wiley-Interscience, New York, pp. 53–126.
25. Skou, J. C., and M. Esmann. 1979. Preparation of membrane-bound and of solubilized ($Na^+ + K^+$)-ATPase from rectal glands of *Squalus acanthias*. The effect of preparative procedures on purity, specific and molar activity. *Biochim. Biophys. Acta.* 567:436–444.
26. Esmann, M. 1988. ATPase and phosphatase activity of Na^+,K^+-ATPase: molar and specific activity, protein determination. *Methods Enzymol.* 156:105–115.
27. Esmann, M., and D. Marsh. 1985. Spin-label studies on the origin of the specificity of lipid-protein interactions in Na^+,K^+-ATPase membranes from *Squalus acanthias*. *Biochemistry.* 24:3572–3578.
28. Fodor, E., N. U. Fedosova, …, M. Esmann. 2008. Stabilization of Na,K-ATPase by ionic interactions. *Biochim. Biophys. Acta.* 1778: 835–843.
29. Bligh, E. G., and W. J. Dyer. 1959. A rapid method of total lipid extraction and purification. *Can. J. Biochem. Physiol.* 37:911–917.
30. Erilov, D. A., R. Bartucci, …, L. Sportelli. 2005. Water concentration profiles in membranes measured by ESEEM of spin-labeled lipids. *J. Phys. Chem. B.* 109:12003–12013.
31. Fauth, J. M., A. Schweiger, …, R. R. Ernst. 1986. Elimination of unwanted echoes and reduction of dead time in 3-pulse electron spin-echo spectroscopy. *J. Magn. Reson.* 66:74–85.
32. Bartucci, R., R. Guzzi, …, D. Marsh. 2009. Intramembrane water associated with TOAC spin-labeled alamethicin: electron spin-echo envelope modulation by D_2O. *Biophys. J.* 96:997–1007.
33. Esmann, M., A. Watts, and D. Marsh. 1985. Spin-label studies of lipid-protein interactions in (Na^+,K^+)-ATPase membranes from rectal glands of *Squalus acanthias*. *Biochemistry.* 24:1386–1393.
34. Miyazaki, J., K. Hideg, and D. Marsh. 1992. Interfacial ionization and partitioning of membrane-bound local anesthetics. *Biochim. Biophys. Acta.* 1103:62–68.
35. Guzzi, R., R. Bartucci, …, D. Marsh. 2009. Conformational heterogeneity and spin-labeled -SH groups: pulsed EPR of Na,K-ATPase. *Biochemistry.* 48:8343–8354.
36. Marsh, D. 2008. Reaction fields and solvent dependence of the EPR parameters of nitroxides: the microenvironment of spin labels. *J. Magn. Reson.* 190:60–67.
37. Guzzi, R., M. Babavali, …, D. Marsh. 2011. Spin-echo EPR of Na,K-ATPase unfolding by urea. *Biochim. Biophys. Acta.* 1808:1618–1628.
38. Esmann, M., A. Arora, …, D. Marsh. 2006. Structural characterization of Na,K-ATPase from shark rectal glands by extensive trypsinization. *Biochemistry.* 45:954–963.
39. Shinoda, T., H. Ogawa, …, C. Toyoshima. 2009. Crystal structure of the sodium-potassium pump at 2.4 A resolution. *Nature.* 459:446–450.
40. Orientations of Proteins in Membranes (OMP) database. 2013. http://opm.phar.umich.edu/. Accessed August 20, 2014.
41. Lomize, M. A., A. L. Lomize, …, H. I. Mosberg. 2006. OPM: orientations of proteins in membranes database. *Bioinformatics.* 22:623–625.
42. Experimentally Determined Hydrophobicity Scales. 2011. http://blanco.biomol.uci.edu/hydrophobicity_scales.html. Accessed August 20, 2014.
43. Wimley, W. C., T. P. Creamer, and S. H. White. 1996. Solvation energies of amino acid side chains and backbone in a family of host-guest pentapeptides. *Biochemistry.* 35:5109–5124.
44. Pogozheva, I. D., S. Tristram-Nagle, …, A. L. Lomize. 2013. Structural adaptations of proteins to different biological membranes. *Biochim. Biophys. Acta.* 1828:2592–2608.
45. Cieslak, J. A., P. J. Focia, and A. Gross. 2010. Electron spin-echo envelope modulation (ESEEM) reveals water and phosphate interactions with the KcsA potassium channel. *Biochemistry.* 49:1486–1494.
46. Delano, W. L. 2002. The Pymol molecular graphics system. DeLano Scientific, San Carlos, CA. http://www.pymol.org. Accessed August 20, 2014.